Research Article | Vol. 31, No. 19 / 11 Sep 2023 / Optics Express 31329
Optics EXPRESS

Simple approach for spectral beam combination of narrowband laser sources for spectroscopic applications

HARALD MOSER,[1,2,*] JOHANNES P. WACLAWEK,[1,2] WALTER PÖLZ,[3] AND BERNHARD LENDL[2]

[1] Competence Center CHASE GmbH, 1030 Vienna, Austria
[2] Institute of Chemical Technologies and Analytics, TU Wien - Vienna University of Technology, 1060 Vienna, Austria
[3] OMV R&M GmbH, 2320 Schwechat, Austria
[*] harald.moser@tuwien.ac.at

Abstract: Spectral beam combination of multiple single mode laser sources employing narrowband spectral filters which are arranged on the perimeter of regular polygons is demonstrated. With this simple geometric design, co-alignment and co-propagation of the individual laser beams can be reasonably achieved. Spectroscopic applicability is displayed by spatial filtering, mode-matching, and subsequent coupling of the combined beams into a 76 m astigmatic mirror multipass cell.

1. Introduction

In the mid-infrared (mid-IR) part of the electromagnetic spectrum in the range of 4000–400 cm^{-1} (2.5–25 µm), especially small molecules exhibit unique and highly structured absorption features based on fundamental vibrations and associated rotational-vibrational transitions. This "fingerprint region" represents a favorable spectral window to probe many atmospheric and process relevant gases, as well as to perform inherently selective molecular discrimination.

For these sensing applications, a general aim with respect to the ongoing development of spectroscopic light sources is to reduce the linewidth of the emitted radiation to a minimum while achieving a spectral coverage as large as possible. In this context, quantum cascade lasers (QCLs) and interband cascade lasers (ICLs) have evolved as compact, powerful, and efficient mid-IR light sources that are band structure engineered with modern epitaxial growth technologies towards precisely defined output wavelengths. These sources can exhibit narrow linewidth and provide high spectral power density [1,2]. The stringent quality requirements in terms of single mode emission and wavelength stability as needed for trace gas sensing are, however, still only met by predominantly distributed-feedback (DFB)-type QCLs and ICLs [3]. The resulting inherently limited tuning range covering a few wavenumbers is the reason why typically only one analyte can be targeted by a given DFB source.

In the last decade, different strategies were proposed and demonstrated in order to improve the spectral coverage while maintaining the high quality of single-mode emission. Promising results could be achieved by modification of the sampled grating distributed feedback laser architecture with digital concatenated gratings [4], by incorporation of a buried microscopic heater element close to the active region [5], by integration of Vernier-effect distributed Bragg reflectors based on superstructure gratings [6] or by integrating an asymmetric sampled grating distributed feedback tunable laser with an optical amplifier [7]. In contrast to the DFB approach where a fixed emission wavelength is selected by means of an integrated Bragg grating, the widely used external cavity (EC) design facilitates broadband spectral tuning by changing the angle of an external diffraction grating [8,9].

#495505 https://doi.org/10.1364/OE.495505
Journal © 2023 Received 17 May 2023; revised 16 Aug 2023; accepted 17 Aug 2023; published 7 Sep 2023

Optics EXPRESS

On the wafer scale level, QCL arrays in different geometries have been demonstrated [10–13] and employed for spectroscopic applications [14]. Due to the limited demand of such arrays, technological maturity is not advanced enough and the preferred way is to employ individually packaged DFB sources that are then combined with dichroic mirrors or beamsplitters [15,16]. The combination of more than two sources with the use of dichroic optical elements requires special attention to the order in which the light sources are introduced into the optical path sequence ("dichroic ladder") to avoid spectral blocking by the next dichroic element in the ladder design [17,18]. While spectral beam blocking is not of great concern when resorting to beam splitter trains, the total light throughput is an important factor to consider, as each beamsplitter considerably decreases the total light output of the system [19]. Moreover, detrimental side effects of lateral displacement, ghosting and fringing are reported, negatively impacting the spectroscopic usability.

2. Overview of beam combination techniques and spatial filtering

Meeting the demanding specifications of extended spectral bandwidth, power and laser beam parameters is generally very complicated to achieve with a single source alone. One potential solution involves combining the beams of several individual laser modules to form a single beam. This is possible to achieve through either coherent or incoherent beam combination techniques.

Coherent beam combination techniques combine the output of several laser sources via constructive interferences and hence tight phase control is mandatory in order to overlap the combined beams [20].

Conversely, incoherent beam combination (IBC, also termed spectral or wavelength beam combination) is an additive superposition without interference of the beams, and thus it does not depend on mutual coherence. IBC methods further include polarization combining, where two beams of mutually orthogonal polarization states are combined into a single beam with high efficiency, but this technique is limited to two beams [21]. In general, IBC has the advantage of avoiding the requirement for polarization, wavelength control, and input phasing, which represents the most complex component. Also, the simplified optical architecture is reflected in the overall robustness and compactness of the system. Moreover, the light intensity distribution in the combined beam is not modified.

In practice, the beams of individual emitters with preferably non-overlapping optical emission spectra are collimated, co-propagated and subsequently co-aligned by employing wavelength-sensitive beam combination elements, such as prisms, beam splitters, diffraction gratings, dichroic mirrors, external cavities, or volume Bragg gratings [22–25].

Traditionally, combining more than two sources with the use of dichroic ladders requires attention to the order in which the light sources are introduced into the optical path sequence to avoid spectral blocking by the next dichroic element in the ladder design [17,18]. While spectral beam blocking is not of great concern when resorting to beam splitter trains, the total light throughput is an important factor, as each beamsplitter considerably decreases the total light output of the system [19]. Moreover, detrimental side effects of ghosting, lateral beam displacement and fringing are reported, negatively impacting the spectroscopic usability.

Addressing the important aspect of beam shape, the rectangular cross section in company with the overall small physical size (typically 10 µm x 25 µm) of the active region of DFB QCL and ICL designs, lead to non-Gaussian near and far field beam profiles [26]. Hence it is desirable to employ spatial filtering in order to transform the output of a non-ideal laser source into a well-defined spatial intensity distribution of Gaussian nature, enabling the subsequent efficient implementation of necessary optical systems.

In the most basic spatial filter configuration, two plano-convex lenses and one pinhole are used within a refracting telescope configuration. The correct focal lengths and pinhole diameter depend on the input wavelength, source beam diameter, and desired exit beam diameter. However,

Optics EXPRESS

when different source beams of vastly different central emission wavelengths are to be combined and introduced into a common refractive spatial filter system, chromatic aberrations in the form of lateral color (transverse chromatic aberrations) and chromatic focal shifts (longitudinal chromatic aberrations) will occur, thus having detrimental effects on the system. Since different wavelengths exhibit different rates of refraction in a given optical material, different angles of divergence emanate from a single refractive surface, leading to significant wavelength spreading.

In order to mitigate the disadvantages of a refractive spatial filter system, reflective optics are the better means of choice. Using pairs of carefully selected off-axis parabolic (OAP) mirrors with suitable focal lengths, chromatic aberrations can be significantly reduced.

3. Optical design of beam combination with narrowband spectral filters

This work reports on a viable alternative to the popular beam splitter train, or dichroic ladder configuration, as encountered in many spectroscopic applications in order to combine multiple individual laser emitters.

The proposed beam combination method utilizes a geometric arrangement of individual narrowband spectral filter (NBSF) elements on the perimeter of regular (i.e., equilateral and equiangular) polygons of odd order. Three examples for such an arrangement (triangle, pentagon and heptagon) are sketched in (Fig. 1(A)). The optimum order is dependent on the total number of individual emitters, and also the incidence angle (α) should be taken into consideration.

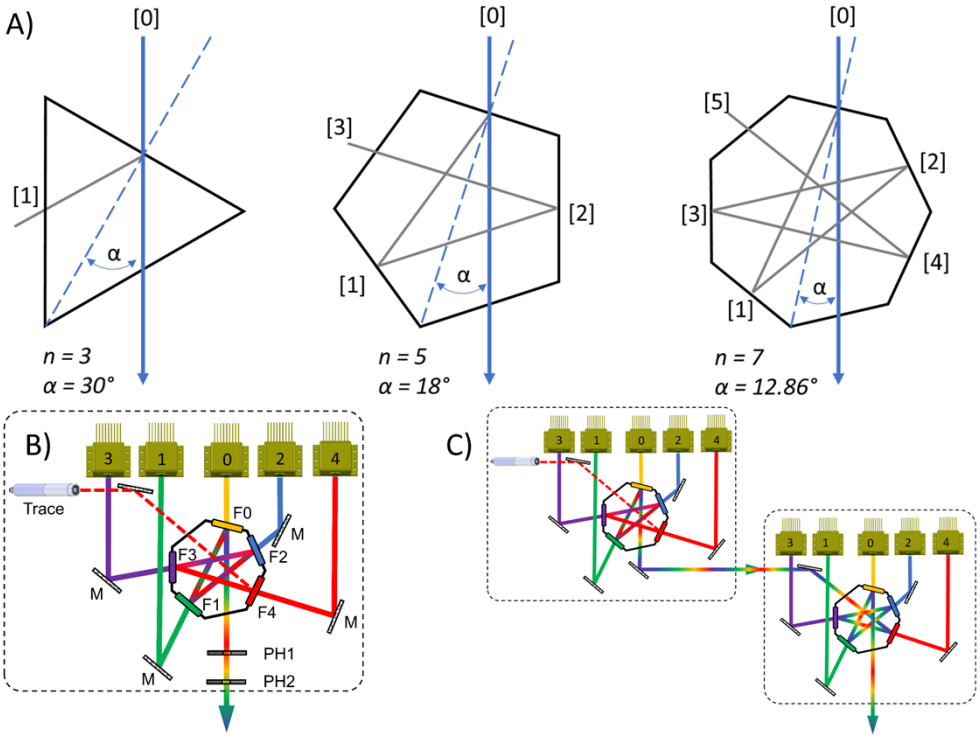

Fig. 1. (A) Sketch of polygons of odd order n = 3 (triangle), 5 (pentagon) and 7 (heptagon). (B) Heptagon layout with 5 + 1 possible laser sources. F: filters, M: steering mirrors in Z-fold configuration, PH: pinhole. (C) Extension of spectral bandwidth with a cascaded layout.

Optics EXPRESS

As opposed to resonant, even-order polygonal, multi-facet resonators [27], the thin-film, hard-coated narrowband spectral filters form non-resonant conditions for the combined laser beams. The individual filters transmit the specified wavelength band ($T > 0.8$), while effectively reflecting ($R>>0.95$) out-of-band emission and blocking and unwanted radiation.

The first filter position (marked as [0] in Fig. 1(A)) is characterized by exclusive transmission of the matching emission source. Without subsequent reflective sequences, this position could be reserved for the emission source with weakest optical power, or the greatest desired output, respectively.

While the position of the last laser on the polygon of odd order is acting as the output with no reflecting surface (i.e., position [3] for the case of a pentagon arrangement) and no filter element is basically required, the remaining positions define the number of reflections of the total optical path. The filter of the last light source (penultimate position, highest number of reflections) is not used as a reflective surface and can be omitted. This position is intended for the use of the most powerful source or can be used as the input port for a visible trace laser, or even used as the re-injection port of cascaded polygon layouts as sketched in Fig. 1(C). The intermediate positions along the perimeter of the odd polygon fill up the missing number of reflections.

Due to the inherent tilt of the filter surface with respect to the optical axis (denoted as α, Fig. 1(A)), direct back reflections to the laser facet are effectively excluded. As a consequence, though, the angle dependent spectral shift of the filter transmission spectrum has to be taken into account and careful selection has to be considered.

The highly flexible nature of the polygon design permits simple configuration changes with the sequence of the employed filters and thus also a total redesign of needed spectral bandwidth can be achieved with minimum effort. Moreover, an extension of spectral bandwidth can be achieved with cascaded layouts.

Fine tuning of the co-alignment and co-propagation of each emitter is realized with the aid of two steering mirrors, aligned in a vertical Z-fold configuration and with placement of two pinholes in the center axis along the final optical path, see Fig. 1(B). The initially misaligned individual laser beams are iteratively and consecutively re-aligned to exactly match the trajectory given by the two pinholes by carefully adjusting pitch and yaw (tilt) of the first mirror (primarily affecting position) and second mirror (change of angle). By iterative re-adjusting position and angle of every emitter beam, final convergence to the central trajectory can be typically achieved after a few tens of re-iterations.

4. Demonstration of spectroscopic application

In a first spectroscopic demonstration, three individual mid-IR QCLs and one visible 635 nm trace diode laser are combined by arranging the emitters along with the matching hard-coated bandpass filters into a regular pentagon. The compact 30 mm optical cage system compatible design was 3D printed by a semi-professional FDM printer (E2, *Raise3D*).

The schematic sketch of the pentagon arrangement and the CAD model of the final assembled optical train is depicted in Fig. 2. In addition, the combined laser beam is further split into an reference and measurement path at the position of a beamsplitting element, marked “BS” in Fig. 2.

Information of the employed laser sources can be found in Table 1 and the according current-to-power and current-to-wavelength data is plotted in Fig. 3. Information regarding the matching narrowband spectral filters (FB series, *Thorlabs*) in terms of central wavelength (CWL) and filter bandwidth half-width at half-maximum (HWHM) is listed in Table 2. The according filter transmission characteristics in combination with the tuning ranges of the designated QCLs are visualized in Fig. 4.

Prior to spectral beam combination, each mid-infrared laser source was investigated in terms of beam quality factor (M^2), which is an important criterium for evaluating subsequential beam

Optics EXPRESS

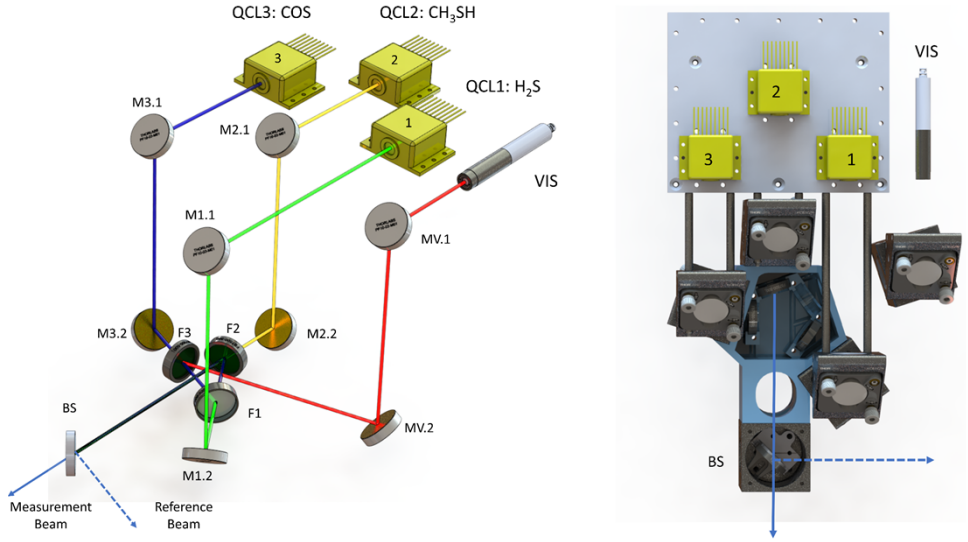

Fig. 2. Schematic sketch (left) and simplified CAD model of the optical train (right). M: mirrors, F: filters, BS: beamsplitter. The combined laser beam is further split into a reference and measurement path at the position of the beamsplitting element.

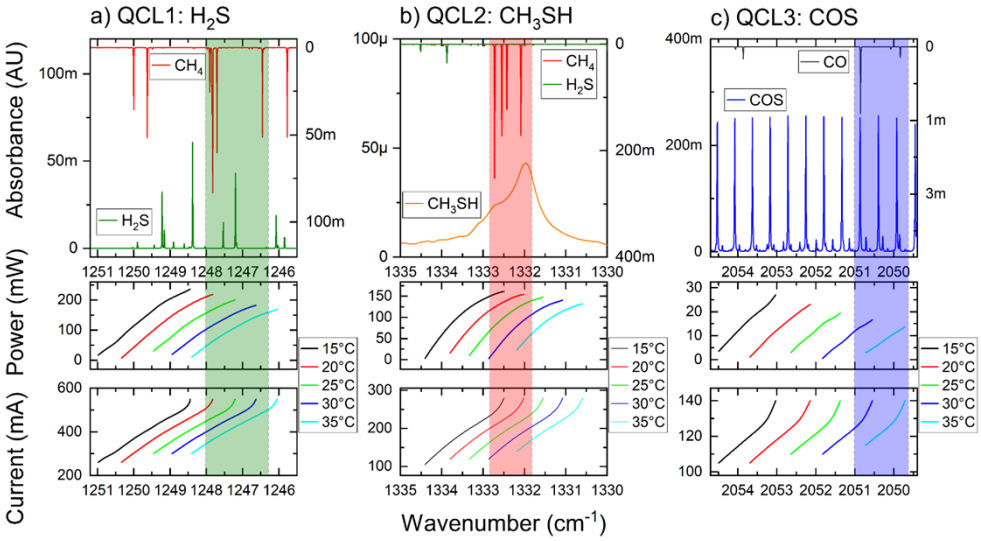

Fig. 3. Laser tuning and optical power parameters along with the designated analyte spectra of H_2S (a), CH_3SH (b) and COS (c). In the top figures absorbance data of the analyte (bottom) and the according reference gas cell constituent (top) is plotted.

Table 1. Employed sources for spectroscopic demonstration.

Source	Manufacturer	ID	Wavelength (µm)	Optical Power (mW)
QCL 1	AdTech	CM7-12-CI0329	8.01	250
QCL 2	Thorlabs	HZ-HHL-0170	7.5	150
QCL 3	Alpes	SBCW8283-HHL	4.7	30
VIS	Thorlabs	PL202	0.635	1

Optics EXPRESS

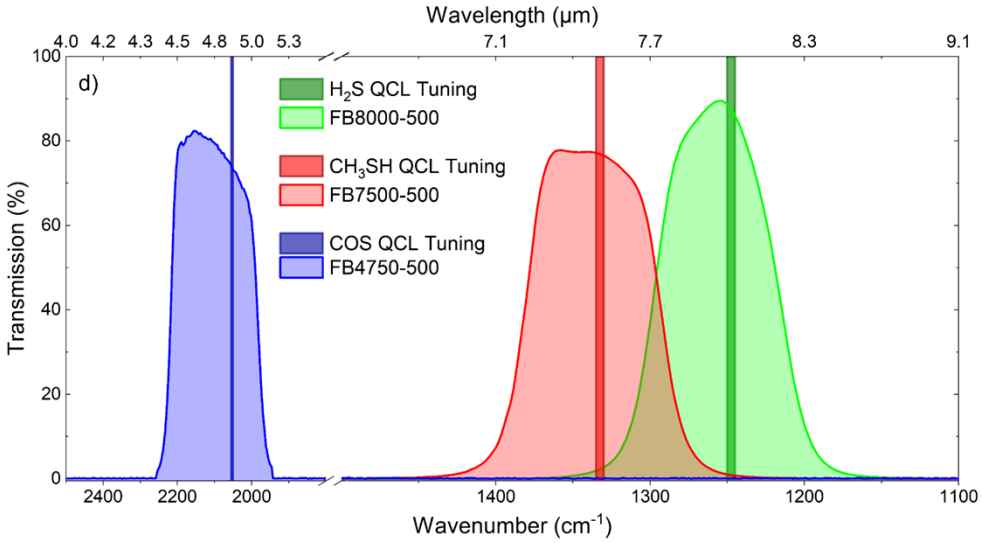

Fig. 4. Spectral transmission characteristics of the employed narrowband filters along with the designated laser tuning ranges.

Table 2. Employed narrowband spectral filters for spectroscopic demonstration.

Source	Filter	Filter CWL (µm)	Filter HWHM (nm)	Transmission (%)	Out-of-Band Reflection (%)
QCL 1	FB 8000 - 500	8.00	500	~85	99.95
QCL 2	FB 7500–500	7.5	500	~75	99.99
QCL 3	FB 4750 - 500	4.75	500	~75	99.9
VIS	(-)	(-)	(-)	(-)	(-)

combination efforts. Beam diameters of the fast and slow axis are evaluated from a series of beam profile measurements along the propagation axis starting at the laser facet (Fig. 5(a)), with a broadband pyroelectric array camera with 80 µm x 80 µm pixel resolution (Pyrocam III HR, *Ophir-Spiricon*). Similar to the individual QCL beam measurements, the beam profiling of the spectrally combined beams is referenced to the positions of the last filter in the system (Fig. 5(b)). The resulting second moment widths (D4σ) of the beam diameters are subsequently least-square fitted to the caustics as specified in ISO 11146:1:2021. The parameters M^2, beam waist diameter ($d0$), beam waist location (z_0), Rayleigh length (z_R) and divergence angle (Θ) are extracted with a modified Python program as introduced by [28] and are summarized in Table 3. More details of the individual beam size measurements and parameter extraction can be found in Supplement 1.

Table 3. Beam quality and propagation parameters

Source	Beam Quality Factor M_X^2 || M_Y^2	Beam Waist Diameter $d0_X$ || $d0_Y$ (mm)	Beam Waist Location $z0_X$ || $z0_Y$ (mm)	Rayleigh Length z_{RX} || z_{RY} (mm)	Divergence Angle Θ_X || Θ_Y (mrad)
QCL 1	1.05 || 1.03	1.37 || 1.44	384 || 248	187 || 212	7.32 || 6.81
QCL 2	1.06 || 1.15	1.64 || 1.61	319 || 382	265 || 236	6.19 || 6.83
QCL 3	1.15 || 1.13	1.32 || 1.13	332 || 440	302 || 225	4.39 || 5.05
Combined	1.35 || 1.26	1.648 || 1.68	164 || 22	211 || 235	7.82 || 7.15

Optics EXPRESS

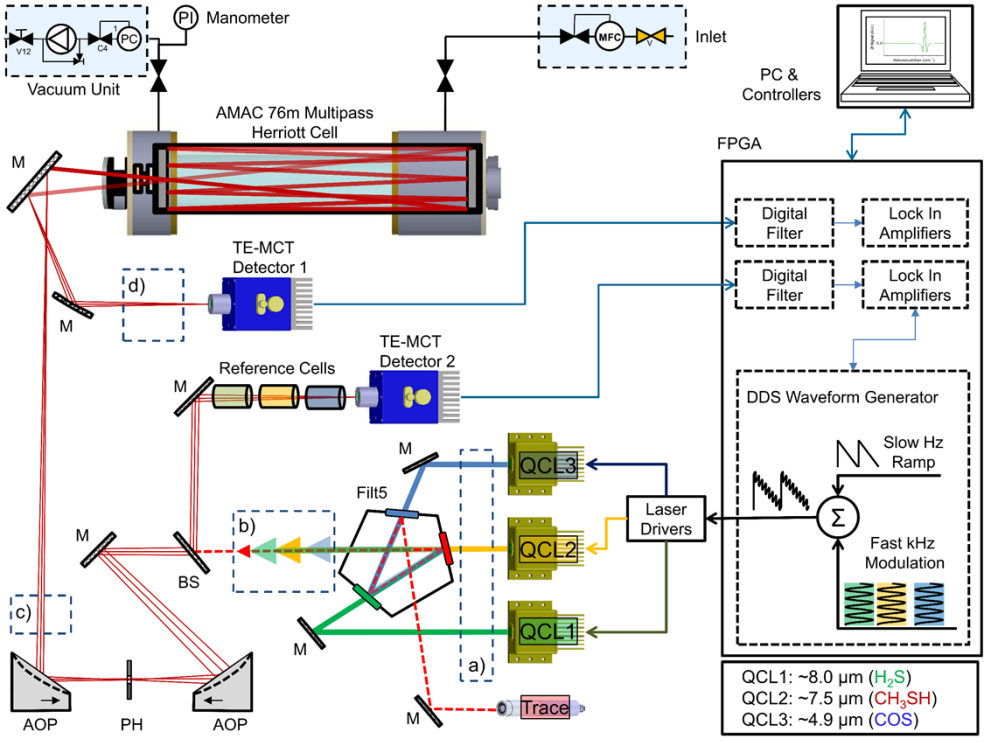

Fig. 5. Optical and peripheral layout for spectroscopic demonstration. The position marks (a)-(d) specify the exemplary recorded beam profiles as plotted in Fig. 6.

M^2 values of the individual QCLs are in the range of 1.1, indicating promising results for the planned beam combination effort. However, due to the different beam waist locations (z0) and Rayleigh lengths (z_R), and the geometrical constraints in terms of total pathlength as a function of the total number of reflections inside the pentagon arrangement, the M^2 values of the combined beam are slighty deteriorated and are found to be in the range of 1.3.

The applicability of the beam combiner was tested within a direct absorption spectroscopy setup previously designed with conventional beamsplitter arrangements [15]. The schematic of the sensor architecture is depicted in Fig. 5. For this purpose, the resulting co-aligned laser beam is split into a reference and signal path before being spatially filtered, mode matched, and coupled into an astigmatic 76 m Herriott multipass cell (AMAC76-LW, *Aerodyne Inc.*). The exiting beam is subsequently focused onto an optically immersed, thermoelectrically cooled MCT detector (PVI-4TE-12, *Vigo Systems*). The reference path is equipped with methane (CH_4), hydrogen sulfide (H_2S) and carbon monoxide (CO) reference gas cells for accurate wavelength calibration and laser drift compensation. The detector signals are digitized, demodulated and further processed using a self-developed multi-channel filtering and lock-in amplifier chain implemented in FPGA hardware (NI 7856R, *National Instruments*).

Exemplary beam profiles at different positions along the optical processing sequence (denoted (a)-(d) and marked in Fig. 5) are displayed in Fig. 6. Beam diameter metrics in terms of D4σ widths in both axes along the optical processing positions are given in Table 4.

Spatial filtering in combination with beam size reduction and subsequent mode-matching to the cell mirror curvature was achieved in a telescopic OAP mirror arrangement with a focal length ratio of 50.8 mm/76.2 mm and a pinhole diameter of 500 µm (Fig. 6(c)). The beam diameter could be moderately reduced to 1.4 mm, ensuring no beam clipping at the cell input coupling

Optics EXPRESS

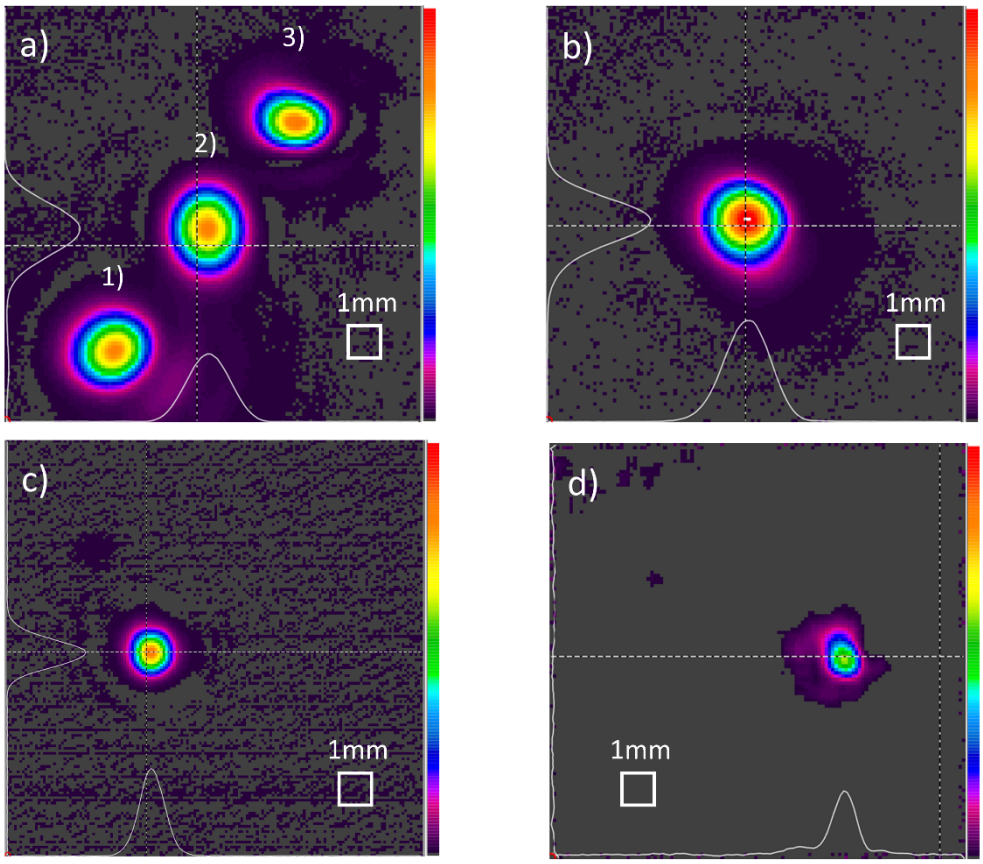

Fig. 6. Beam profiles at marked positions along the optical processing sequence (refer to Fig. 5). (a) Individual beam profiles of the single laser sources: QCL1, lower left, QCl2, middle and QCL3 top right. (b) Beam profile after co-alignment. (c) Beam profile after spatial filtering and telescopic beam size reduction with f = 50.8 mm/76.2 mm and pinhole diameter of 500 µm. (d) Beam profile after 76 m propagation inside multipass cell.

Table 4. D4σ widths along the optical processing positions.

	D4σ beam diameters in X and Y-axis, D4σX || D4σY (mm)			
Position	QCL1	QCL2	QCL3	Beam Combination
a	2.6 | 2.3	2.4 | 2.6	2.3 | 1.9	
b				2.6 | 2.6
c				1.4 | 1.4
d				1.2 | 1.4

hole with a diameter of 4.3 mm. The beam profile after 76 m propagation length inside the multipass cell (Fig. 6(d)) revealed limited deviation from ideal gaussian intensity distribution and spatial separation of the individual beams, substantiating the efficacy of the co-alignment, spatial filtering and mode-matching efforts.

Quantitative measurements of 10 ppmV H_2S, 1.0 ppmV CH_4 and 500 ppbV COS, were performed using calibration gas mixtures in nitrogen (N_2), in order to investigate the sensitivity and assess the baseline fringe level of the employed NBSF setup. The specific target analyte

Optics EXPRESS

concentration levels were prepared by 5.0 N_2 (99.999%) dilution from standardized gas bottles (matrix N_2) with a mass flow and pressure controlled in house developed gas handling system. Pressure monitoring was performed with a digital manometer (Leo3, *Keller*). The multipass cell was operated at room temperature (295 ± 2.5 K), at flow rates ranging from 0.1 to 1.0 l/min and at total pressures ranging from 15 mbar to 100 mbar in order to spectrally resolve the ro-vibrational bands of the designated analyte molecules. The results are visualized in Fig. 7 and indicate promising performance in terms of signal-to-noise ratio and baseline fringe levels for sensitive and selective metrological task with demand of sub-ppmV resolution.

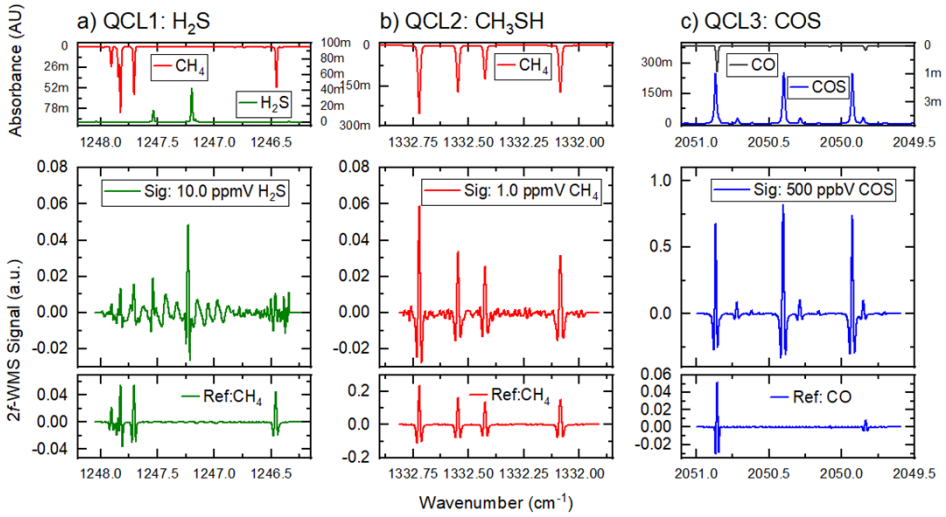

Fig. 7. Quantitative measurements of 10 ppmV H_2S, 1.0 ppmV CH_4 and 500 ppbV COS. The multipass cell was operated at room temperature (295 ± 2.5 K), at flow rates ranging from 0.1 to 1.0 l/min and at total pressures ranging from 15 mbar to 100 mbar. In the top figures absorbance data of the analyte and the according reference gas cell constituent is plotted. Power normalized second harmonic wavelength modulation (2*f*-WMS) data is plotted for both signal (middle) and reference path (lower).

5. Comparison of different beam combination setups

The beam combination efficiency of the proposed narrowband spectral filter (NBSF) architecture is compared with three different beams splitter configurations. The two plate beamsplitters are front coated with a ZnSe and CaF_2 surface, respectively which determine the beam splitting ratio. The third type of beamsplitter is a pellicle beamsplitters (PBS) manufactured from an extremely thin (few microns thick) and thus fragile nitrocellulose membrane. PBS design are considered ideal for use in applications where chromatic dispersion must be minimized and focused beams are necessary. Detailed listing of the wavelength dependent transmission and reflection ratios together with the relevant manufacturer information can be found in Table S1 in Supplement 1. The comparison of overall beam combination efficiencies for different beam combination architectures is listed in Table 5. Further details of the optical manipulation sequences in terms of number of transmissions and reflections along with the wavelength dependent efficiencies for each beam combination setup can be found in Table S2 in Supplement 1.

Resorting to traditional plate beamsplitters, it is evident that great care of selecting the most suitable coating along with a carefully selected sequence of optical manipulation in terms of transmission and reflection for each spectroscopic source must be taken into account. While it is desirable to maximize optical power in the signal path after beam combination, geometrical

Optics EXPRESS

Table 5. Comparison of overall beam combination efficiencies for different beam combination architectures.

	Beam combination efficiency for signal and refence path (%)			
	NBSF	ZnSe	CaF2	PBS
QCL1	75 || 9.8	11.9 || 4.7	20.1 || 10.6	3 || 0.15
QCL2	69.6 || 5.4	31.1 || 12	40.8 || 19.9	49.9 || 5.9
QCL3	71.7 || 3.1	20.1 || 60.1	36.1 || 62.1	24.6 || 64.6

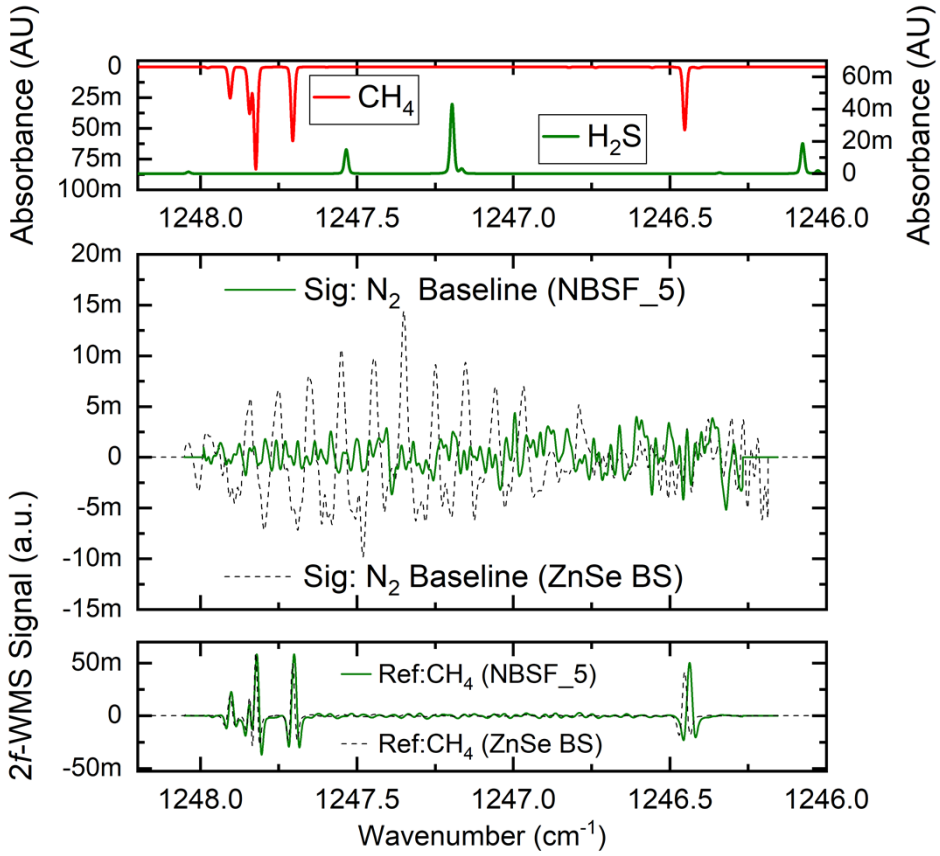

Fig. 8. Direct comparison of NBSF setup with a traditional ZnSe beamsplitter ladder. The maximum peak-to-peak fringe baseline level in the signal path (middle) could be reduced by a factor of ~3.

constraints regarding placement of laser sources and overall compactness of the optical train lead to unsatisfactory conditions and compromises have to be made, leading to unbalanced spectroscopic requirements. The vastly different efficiencies for both plate beamsplitter options in the case of beam combination of three different QCLs seem to reflect the necessity of meticulous design. For example, QCL3 exhibits more than 60% of the initial optical power in the reference path for both plate beamsplitter options. In this case, redesign of the optical train in order to relocate more power to the signal path would be necessary.

Optics EXPRESS

The unbalanced nature for PBS designs seems to very evident in the case of the first laser source (QCL1). In this specific case, an efficiency of only 3% of the initial optical power can be anticipated in the signal path.

In light of overall efficiency and ease of implementation in preexisting optical trains, the NBSF setup seems to be a valid and feasible alternative to traditional beam splitter designs. The main advantages of employing NBSF are their intrinsic high initial transmission ratio in excess of 70%, paired with very high reflectivity (R > 99.9%) of out-of-band radiation. As a result, no particular care has to be taken into account in design of the most suitable optical sequence. The combined laser beams will exhibit comparable losses in terms of initial laser power and when using a thin, uncoated CaF_2 window for splitting the beam into a signal and reference line, power levels of ~70-75% and ~3-10% can be expected in the signal and reference arm, respectively.

A direct comparison of the proposed NBSF setup with a traditional ZnSe beamsplitter ladder is visualized in Fig. 8. In this context it is worth mentioning that the NBSF setup could considerably improve the fringe baseline level in comparison with the traditional ZnSe optics. In particular, the maximum peak-to-peak fringe baseline level in the signal path could be reduced by a factor of ~3 and a direct improvement in spectroscopic performance can be anticipated.

6. Conclusion

The spectral beam combination of narrowband sources employing narrowband spectral filters (NBSFs) in a polygonal geometric design allows for efficient extension of spectral bandwidth and can be easily implemented for demanding spectroscopic applications. This straightforward method provides flexibility in selecting the desired wavelengths of the individual laser modules and produces a broader spectral output. Furthermore, the reliability and efficiency of spectroscopic laser systems is enhanced, as the combination of discrete laser modules eliminates the need for complex optical components.

The highly flexible nature of the polygon design permits simple configuration changes with the sequence of the employed filters and thus also a total redesign of needed spectral bandwidth can be achieved with minimum effort. Moreover, an extension of spectral bandwidth can be achieved with cascaded layouts.

For the exemplary reported spectroscopic application, the laser beams of three individual QCL module could be co-aligned in a pentagon filter arrangement and subsequently, spatial filtered and mode-matched with the aid of an OAP mirror telescope equipped with a 500 µm pinhole. After coupling the combined beam into a 76 m multipass cell, the beam profile of the exiting beam revealed limited deviation from ideal gaussian intensity distribution and spatial separation of the individual beams, substantiating the efficacy of the co-alignment, spatial filtering and mode-matching efforts. As an added benefit, the the maximum peak-to-peak fringe baseline level in the signal path could be reduced by a factor of ~3 relating to an anticipated direct improvement in spectroscopic performance.

Regarding recent developments in photoacoustic and photothermal laser spectroscopic techniques [29,30] where efficient combination of multiple laser source while maximizing optical power in the signal path is of utmost importance, the beam combination using NBSFs can be anticipated as a feasible alternative to traditional plate beam splitter designs.

Funding. Österreichische Forschungsförderungsgesellschaft (COMET - Competence Center CHASE GmbH).

Acknowledgments. COMET Centre CHASE is funded within the COMET – Competence Centers for Excellent Technologies programme by the BMK, the BMDW and the Federal Provinces of Upper Austria and Vienna. The COMET programme is managed by the Austrian Research Promotion Agency (FFG).

Disclosures. The authors declare no conflicts of interest.

Data availability. Data underlying the results presented in this paper are not publicly available at this time but may be obtained from the authors upon reasonable request.

Optics EXPRESS

Supplemental document. See Supplement 1 for supporting content.

References

1. J. Meyer, W. Bewley, C. Canedy, C. Kim, M. Kim, C. Merritt, and I. Vurgaftman, "The Interband Cascade Laser," Photonics **7**(3), 75 (2020).
2. M. S. Vitiello, G. Scalari, B. Williams, and P. De Natale, "Quantum cascade lasers : 20 years of challenges," Opt. Express **23**(4), 5167–5182 (2015).
3. J. Faist, C. Gmachl, F. Capasso, C. Sirtori, D. L. Sivco, J. N. Baillargeon, and A. Y. Cho, "Distributed feedback quantum cascade lasers," Appl. Phys. Lett. **70**(20), 2670–2672 (1997).
4. S. Slivken, N. Bandyopadhyay, Y. Bai, Q. Y. Lu, and M. Razeghi, "Extended electrical tuning of quantum cascade lasers with digital concatenated gratings," Appl. Phys. Lett. **103**(23), 1 (2013).
5. A. Bismuto, Y. Bidaux, C. Tardy, R. Terazzi, T. Gresch, J. Wolf, S. Blaser, A. Muller, and J. Faist, "Extended tuning of mid-ir quantum cascade lasers using integrated resistive heaters," Opt. Express **23**(23), 29715 (2015).
6. Y. Bidaux, A. Bismuto, C. Tardy, R. Terazzi, T. Gresch, S. Blaser, A. Muller, and J. Faist, "Extended and quasi-continuous tuning of quantum cascade lasers using superstructure gratings and integrated heaters," Appl. Phys. Lett. **107**(22), 29715–29722 (2015).
7. S. Slivken, S. Sengupta, and M. Razeghi, "High power continuous operation of a widely tunable quantum cascade laser with an integrated amplifier," Appl. Phys. Lett. **107**(25), 251101 (2015).
8. K. Knabe, P. a Williams, F. R. Giorgetta, C. M. Armacost, S. Crivello, M. B. Radunsky, and N. R. Newbury, "Frequency characterization of a swept- and fixed-wavelength external-cavity quantum cascade laser by use of a frequency comb," Opt. Express **20**(11), 12432 (2012).
9. T. Vahlsing, H. Moser, M. Grafen, K. Nalpantidis, M. Brandstetter, H. M. Heise, B. Lendl, S. Leonhardt, D. Ihrig, and A. Ostendorf, "Mid-infrared spectroscopic characterisation of an ultra-broadband tunable EC-QCL system intended for biomedical applications," in *European Conferences on Biomedical Optics*, J. Q. Brown and V. Deckert, eds. (2015), Vol. 9537, p. 953713.
10. B. G. Lee, M. A. Belkin, C. Pflugl, L. Diehl, H. A. Zhang, R. M. Audet, J. MacArthur, D. P. Bour, S. W. Corzine, G. E. Hufler, and F. Capasso, "DFB Quantum Cascade Laser Arrays," IEEE J. Quantum Electron. **45**(5), 554–565 (2009).
11. P. Rauter and F. Capasso, "Multi-wavelength quantum cascade laser arrays," Laser Photon. Rev. **9**(5), 452–477 (2015).
12. F. Kapsalidis, M. Shahmohammadi, M. J. Süess, J. M. Wolf, E. Gini, M. Beck, M. Hundt, B. Tuzson, L. Emmenegger, and J. Faist, "Dual-wavelength DFB quantum cascade lasers: sources for multi-species trace gas spectroscopy," Appl. Phys. B **124**(6), 107 (2018).
13. E. Mujagić, C. Schwarzer, Y. Yao, J. Chen, C. Gmachl, and G. Strasser, "Two-dimensional broadband distributed-feedback quantum cascade laser arrays," Appl. Phys. Lett. **98**(14), 141101 (2011).
14. H. Moser, A. Genner, J. Ofner, C. Schwarzer, G. Strasser, and B. Lendl, "Application of a ring cavity surface emitting quantum cascade laser (RCSE-QCL) on the measurement of H_2S in a CH_4 matrix for process analytics," Opt. Express **24**(6), 6572 (2016).
15. H. Moser, J. P. Waclawek, A. Genner, C. Gasser, and B. Lendl, "A triple quantum cascade laser based sulfur species sensor for H2S, CH3SH and COS in petrochemical process streams," in *Conference on Lasers and Electro-Optics* (Optical Society of America, 2018), paper AM2M.7.
16. A. Genner, P. Martín-mateos, H. Moser, and B. Lendl, "A quantum cascade laser-based multi-gas sensor for ambient air monitoring," Sensors **20**(7), 1850 (2020).
17. J. B. McManus, M. S. Zahniser, D. D. Nelson, J. H. Shorter, S. Herndon, E. Wood, and R. Wehr, "Application of quantum cascade lasers to high-precision atmospheric trace gas measurements," Opt. Eng. **49**(11), 111124 (2010).
18. B. Bereiter, B. Tuzson, P. Scheidegger, A. Kupferschmid, H. Looser, L. Machler, D. Baggenstos, J. Schmitt, H. Fischer, and L. Emmenegger, "High-precision laser spectrometer for multiple greenhouse gas analysis in 1 mL air from ice core samples," Atmos. Meas. Tech. **13**(11), 6391–6406 (2020).
19. M. Müller, C. Aleshire, J. Buldt, H. Stark, C. Grebing, A. Klenke, and J. Limpert, "Scaling potential of beam-splitter-based coherent beam combination," Opt. Express **29**(17), 27900 (2021).
20. C. L. Linslal, P. Ayyaswamy, S. Maji, M. S. Sooraj, A. Dixit, D. Venkitesh, and B. Srinivasan, "Challenges in coherent beam combining of high power fiber amplifiers: a review," ISSS J. Micro Smart Syst. **11**(1), 277–293 (2022).
21. S. Li, Z. Wu, F. Wu, G. Zhou, X. Bi, C. An, Q. Liu, R. Yang, J. Wang, Y. Li, J. Cai, and X. Yan, "Incoherent polarization beam combination for mid-infrared semiconductor lasers," in *14th National Conference on Laser Technology and Optoelectronics*, H.-L. Xu, F. Chen, and L. Ji, *et al.*, eds. (SPIE, 2019), p. 178.
22. B. Mroziewicz and E. Pruszyńska-Karbownik, "On the beam radiance of mid-infrared quantum cascade lasers–A review," Opto-Electron. Rev. **27**(2), 161–173 (2019).
23. H. Fathi, M. Närhi, and R. Gumenyuk, "Towards ultimate high-power scaling: Coherent beam combining of fiber lasers," Photonics **8**(12), 566 (2021).
24. B. G. Lee, J. Kansky, A. K. Goyal, C. Pflügl, L. Diehl, M. a Belkin, A. Sanchez, and F. a Capasso, "Beam combining of quantum cascade laser arrays," Opt. Express **17**(18), 16216–24 (2009).
25. S. Hugger, F. Fuchs, R. Aidam, W. Bronner, R. Loesch, Q. Yang, N. Schulz, J. Wagner, E. Romasew, M. Raab, and H. D. Tholl, "Spectral beam combining of quantum cascade lasers in an external cavity," Laser Technol. Def. Secur. V **7325**, 73250H (2009).

Optics EXPRESS

26. K. Krishnaswami, B. E. Bernacki, B. D. Cannon, N. Hô, and N. C. Anheier, "Emission and propagation properties of midinfrared quantum cascade lasers," IEEE Photonics Technol. Lett. **20**(4), 306–308 (2008).
27. A. K. Bhowmik, "Polygonal optical cavities," Appl. Opt. **39**(18), 3071 (2000).
28. S. Prahl, "Laser Beam Size @ github.com/scottprahl/laserbeamsize," (2023).
29. J. P. Waclawek, H. Moser, and B. Lendl, "Balanced-detection interferometric cavity-assisted photothermal spectroscopy employing an all-fiber-coupled probe laser configuration," Opt. Express **29**(5), 7794 (2021).
30. A. Sampaolo, P. Patimisco, M. Giglio, A. Zifarelli, H. Wu, L. Dong, and V. Spagnolo, "Quartz-enhanced photoacoustic spectroscopy for multi-gas detection: A review," Anal. Chim. Acta **1202**, 338894 (2022).